Statistical characterization of microstructure of packings of polydisperse hard cubes

Hessam Malmir and Muhammad Sahimi*
Mork Family Department of Chemical Engineering and Materials Science, University of Southern California, Los Angeles, California 90089-1211, USA

M. Reza Rahimi Tabar
Department of Physics, Sharif University of Technology, Tehran 11365-9161, Iran
(Received 8 January 2017; published 22 May 2017)

Polydisperse packings of cubic particles arise in several important problems. Examples include zeolite microcubes that represent catalytic materials, fluidization of such microcubes in catalytic reactors, fabrication of new classes of porous materials with precise control of their morphology, and several others. We present the results of detailed and extensive simulation and microstructural characterization of packings of nonoverlapping polydisperse cubic particles. The packings are generated via a modified random sequential-addition algorithm. Two probability density functions (PDFs) for the particle-size distribution, the Schulz and log-normal PDFs, are used. The packings are analyzed, and their random close-packing density is computed as a function of the parameters of the two PDFs. The maximum packing fraction for the highest degree of polydispersivity is estimated to be about 0.81, much higher than 0.57 for the monodisperse packings. In addition, a variety of microstructural descriptors have been calculated and analyzed. In particular, we show that (i) an approximate analytical expression for the structure factor of Percus-Yevick fluids of polydisperse hard spheres with the Schulz PDF also predicts all the qualitative features of the structure factor of the packings that we study; (ii) as the packings become more polydisperse, their behavior resembles increasingly that of an ideal system—"ideal gas"—with little or no correlations; and (iii) the mean survival time and mean relaxation time of a diffusing species in the packings increase with increasing degrees of polydispersivity.

DOI: 10.1103/PhysRevE.95.052902

I. INTRODUCTION

This paper is devoted to microstructural characterization of polydisperse packings of hard cubic particles. The study has been motivated by our recent work on the development of a new method of fabrication of porous materials [1]. In this method, a salt, such as NaCl, which consists of cubic crystals and is suspended in a nonsoluble medium, such as an alcohol or ketone, is used to coat a nonporous surface, such as a plastic film, metal foil, or a glass. A polymeric material is then hot-pressed over the salt layer that fills the void space between the salt crystals and solidifies upon cooling. The salt crystals are then washed off with water, creating voids and exposing the pore space. As the melting temperature of most salts is very high, they preserve the shape of their crystals. Thus, their packing retains its microstructure even at the high temperature at which the polymeric material is hot-pressed over the salt layer. The method has the advantage that the size distribution of the salt crystals *before* being hard-pressed by the polymeric material is the same as the *pore-size distribution* of the porous medium *after* the salt crystals are washed off. Thus, one has significant control over the microstructure of the porous medium fabricated by the method.

In addition, packing of cubic particles is encountered in biological materials [2], colloids [3], and other systems of scientific importance. As an important practical example, consider evaporation of saline water in soil [4]. As evaporation proceeds, salt crystallizes and precipitates on the surface of the pores in which the saline water flows, giving rise to a packing of cubic salt crystals that damages the surface and reduces the permeability and porosity of the soil.

In a previous paper [5], hereafter referred to as part I, we defined the essential part of the problem, and we reported some preliminary results. In a subsequent paper [6], which we refer to as part II, we presented the details of the computational algorithm for generating a large packing of cubic particles, the solution of which belongs to a class of problems that are referred to as computationally *hard problems*, and we presented the results for various two-point correlation functions that characterize the packings' microstructure. The computational procedure that we have developed is a modification of the random sequential-addition (RSA) algorithm, which, to our knowledge, had not been developed before. Our study indicated that the maximum packing fraction is ≈ 0.57, representing the boundary between a liquid-crystal phase and a crystalline structure. In addition, we studied the effect of the porosity and finite size of the packings on their characteristics, demonstrating that the packings possess both spatial and orientational long-range order at high packing fractions.

In both parts I and II, we studied packings of cubic particles with equal sizes. In practice, however, the particles or crystals are most likely polydisperse, with their sizes distributed according to a probability density function (PDF). Examples include ceramic powders, paint pigments, and colloidal suspensions. Using polydisperse powders leads to considerable advantages, such as higher packing densities [7] and increased fluidity of concentrated suspensions [8]. While the properties of packings of polydisperse spherical particles have been studied by many researchers [9–26], the same is not true about packings of polydisperse nonspherical

*moe@usc.edu

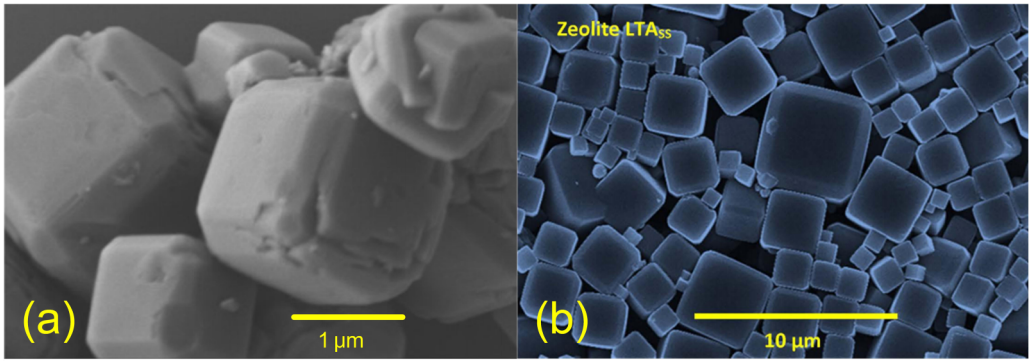

FIG. 1. The SEM images of (a) cubic aluminosilicate zeolite particles (Advera® 401) suspended in a Newtonian fluid of polyethylene glycol (after Ref. [33]), and (b) self-synthesized LTA zeolite crystals (after Ref. [34]).

particles. Desmond and Weeks [19] studied the packing fraction as a function of the polydispersity and skewness of various particle size distributions. Baranau and Tallarek [27] investigated random close packings of polydisperse hard spheres. Furthermore, the effective flow and transport properties of packed beds of polydisperse hard spheres, such as the conductivity and permeability, have been reported in a few studies [28–30]. However, random packings of polydisperse nonspherical particles have rarely been explored.

In the present paper, we report a detailed simulation of random packings of polydisperse hard cubes, as well as an analysis of a variety of microstructural descriptors for such porous materials. The present study, in addition to shedding further light on the properties of packings of cubic particles, also contributes to the more general problem of understanding the properties of polydisperse packings of nonspherical particles. In addition to the aforementioned problem of fabrication of a new class of porous materials, the present study is motivated by other important applications. One example is packings of zeolites, a highly important catalytic material that has been used in the chemical industry for a long time. More recently, zeolites have been proposed [31] for separation of fluid mixtures. They consist of cubic particles [32], an image of which, obtained by a scanning electron microscope, is shown in Fig. 1(a), showing polydisperse aluminosilicate zeolites (Advera®401), suspended in polyethylene glycol [33]. Figure 1(b) shows self-synthesized Linde type A (LTA) zeolite crystals with a variety of sizes [34].

The rest of the paper is organized as follows: In Sec. II, the computational approach for generating random packings of polydisperse cubic particles and the PDFs of the particles' sizes are described. We then present and discuss in Sec. III the results for a variety of the important microstructural descriptors of the packings. Section IV summarizes the paper and discusses possible further research.

II. THE MODEL AND ALGORITHM

The most efficient numerical algorithms for generating packings of hard spheres are a Monte Carlo (MC) method developed by He *et al.* [13], and a modification of the Lubachevsky-Stillinger algorithm [35] developed by Kansal *et al.* [14]. Clusel *et al.* [36] introduced the "granocentric" model for random packing of jammed emulsions by which they simulated random packing of polydisperse frictionless spheres [18], and they investigated the structure of its jamming [20]. However, such methods cannot be used for generating random packings of mono- or polydisperse hard cubes. We also note that various molecular dynamics and MC methods that have been used for generating hard-particle packings are not applicable to packing of cubes, because the overlap potential functions cannot be constructed for particles with nonsmooth shapes, including all the Platonic and Archimedean solids. For such particles, Torquato and Jiao [37,38] developed an optimization algorithm that they referred to as the adaptive shrinking cell (ASC) method, which is based on an MC method with the Metropolis acceptance rule. Except for tetrahedra, packings of other Platonic solids (cube, octahedra, dodecahedra, and icosahedra) generated by the ASC algorithm are their lattice packings. Since a cube is the only Platonic object that tiles the space, its lattice packing generated by the ASC algorithm is highly ordered with densities close to unity [6,37,38]. Delaney and Cleary [39] proposed another algorithm for generating packings of particles, the dynamic particle expansion technique, which was originally developed for the so-called superellipsoids, defined by

$$\left(\frac{x}{a}\right)^p + \left(\frac{y}{b}\right)^p + \left(\frac{z}{c}\right)^p = 1, \tag{1}$$

in which p is a shape parameter, and a, b, and c are the semimajor axes lengths. For large values of p, the particles take on shapes that approach cubes. This method also generates ordered packings of hard cubic particles.

In parts I and II we presented an algorithm that was based on a modification of the RSA process, which is also used in the present paper. The simulation begins with a large, empty region of volume V in $\mathbb{R}^3$, in which cubic particles are inserted with random edge lengths D drawn from a given distribution for the particles' sizes. The cubes are then placed sequentially in the simulation cell at randomly selected positions and orientations, taking into account the nonoverlapping constraint. Adding the particles is continued until the desired packing fraction $\phi = \rho\langle v_1(D)\rangle$ is reached, where $\rho = N/V$ is the total number density, and $\langle v_1(D)\rangle = \langle D^3\rangle$ is the mean volume of the cubic particles.

A. The computational algorithm

The details of the computational algorithm are as follows:

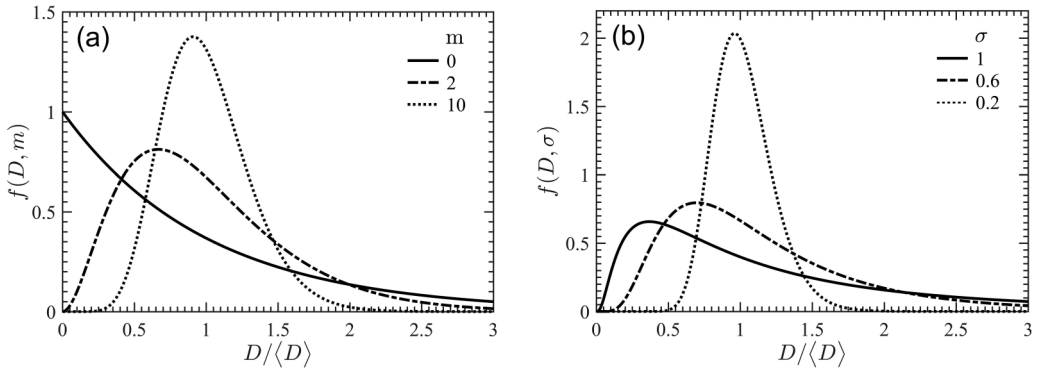

FIG. 2. The size distributions of the particles. (a) The Schulz distribution, and (b) the log-normal distribution.

Step 1. The total number N of cubic particles and the size of the simulation cell, $L_x \times L_y \times L_z$, are specified.

Step 2. The cube's edge length D is selected randomly from a normalized PDF $f(D)$ for the size of the particles.

Step 3. Three random numbers $x_c \in (0,L_x)$, $y_c \in (0,L_y)$, and $z_c \in (0,L_z)$ are generated for the center of a new cubic particle.

Step 4. Two random numbers $u \in [-1,1]$ and $\phi \in [0,2\pi)$ are generated for the normal vector $\mathbf{n}$ of the upper face of the cubes, given by

$$\mathbf{n} = \sqrt{1-u^2}\cos\phi\mathbf{i} + \sqrt{1-u^2}\sin\phi\mathbf{j} + u\mathbf{k}, \tag{2}$$

where $\mathbf{i}$, $\mathbf{j}$, and $\mathbf{k}$ are the three unit vectors in Cartesian coordinates (x,y,z).

Step 5. The matrix $\mathbf{R}$ that rotates the unit vector $\mathbf{k}$ into the unit vector $\mathbf{n}$ through

$$\mathbf{R} = \mathbf{I} + \mathbf{A} + \mathbf{A}^2\frac{(1-\mathbf{k})\cdot\mathbf{n}}{\|\mathbf{v}\|^2} \tag{3}$$

is constructed, where $\mathbf{I}$ is the identity matrix, and the unit vector $\mathbf{v} = (v_1,v_2,v_3)$ is defined by $\mathbf{k}\times\mathbf{n}$. Furthermore,

$$\mathbf{A} = \begin{bmatrix} 0 & -v_3 & v_2 \\ v_3 & 0 & -v_1 \\ -v_2 & v_1 & 0 \end{bmatrix}. \tag{4}$$

Note that if $\mathbf{n} = \mathbf{k}$, then $\mathbf{R} = \mathbf{I}$, and if $\mathbf{n} = -\mathbf{k}$, we have, $\mathbf{R} = -\mathbf{I}$.

Step 6. The coordinates of the cube's eight vertices, $\mathbf{V}_i$, $i = [1,2,\ldots,8]$, are computed by

$$\mathbf{V}_i = \mathbf{V}_{\mathbf{i},\mathbf{n}} + \mathbf{V}_\mathbf{c}, \tag{5}$$

where $\mathbf{V}_c$ is the coordinate vector of the cube's center, and $\mathbf{V}_{i,n} = \mathbf{R}\mathbf{W}_i$, in which $\mathbf{W}_1 = (-d_0/2,-d_0/2,-d_0/2),\ldots,\mathbf{W}_8 = (d_0/2,d_0/2,d_0/2)$.

Step 7. All the cube's vertices are examined to see whether they are outside the previously inserted particles. If so, the new particle is accepted and one increases $n \to n+1$, where n is the current number of accepted particles. If $n \leqslant N$, return to Step 3, or if $n = N$, the simulation is terminated.

B. Particle-size distributions

We utilize two PDFs as the particle-size distribution. One is the Schulz distribution, sometimes referred to as the Schulz-Zimm distribution, which arises in a variety of problems [40–43] and is given by

$$f(D,m) = \frac{1}{\Gamma(m+1)}\left(\frac{m+1}{\langle D\rangle}\right)^{m+1} D^m \exp\left[\frac{-(m+1)D}{\langle D\rangle}\right], \tag{6}$$

where m is an integer in $[0,\infty)$, $\Gamma(x)$ is the Gamma function, and $\langle D\rangle$ is the mean edge length of the cubic particles. The nth moment of the distribution is given by

$$\langle D^n\rangle = \frac{(m+n)!}{m!}\frac{1}{(m+1)^n}\langle D\rangle^n, \tag{7}$$

implying that as m increases, the variance $\langle D^2\rangle - \langle D\rangle^2$ decreases. Hence, $m \to \infty$ represents a monodisperse packing with $\lim_{m\to\infty} f(D,m) = \delta(D - \langle D\rangle)$. Thus, the maximum packing polydispersity is obtained with $m = 0$.

A log-normal particle-size distribution is also encountered in several problems [44–49], and is given by the well-known equation

$$f(D,\sigma) = \frac{1}{D\sigma\sqrt{2\pi}}\exp\left\{\frac{-[\ln(D/\langle D\rangle)]^2}{2\sigma^2}\right\}, \tag{8}$$

in which $\ln D$ is distributed according to a Gaussian PDF, with the mean $\langle D\rangle$ and the standard deviation $\sigma = \sqrt{\langle(\ln D)^2\rangle - \langle\ln D\rangle^2}$. The nth moment of the distribution is given by

$$\langle D^n\rangle = \exp\left(\frac{n^2\sigma^2}{2}\right)\langle D\rangle^n, \tag{9}$$

implying that $\sigma \to 0$ represents the monodisperse packings with $\lim_{\sigma\to 0} f(D,\sigma) = \delta(D - \langle D\rangle)$. Figure 2 presents samples of the two distributions for three values of the parameters m and σ.

III. RESULTS

We assume that the mean edge length of the particles is $\langle D\rangle = 0.05L$, where L is the linear size of the simulation cell. For simplicity, we refer to the pore space and the solid particles as phases 1 and 2, respectively. The porosity and packing density of the system are therefore, respectively, ϕ_1 and ϕ_2. Figure 3 presents the top view of six packings whose sizes are distributed according to the Schulz and log-normal distributions with the packing fraction $\phi_2 = 0.2$. Most of the results presented in this paper are for the packings shown in

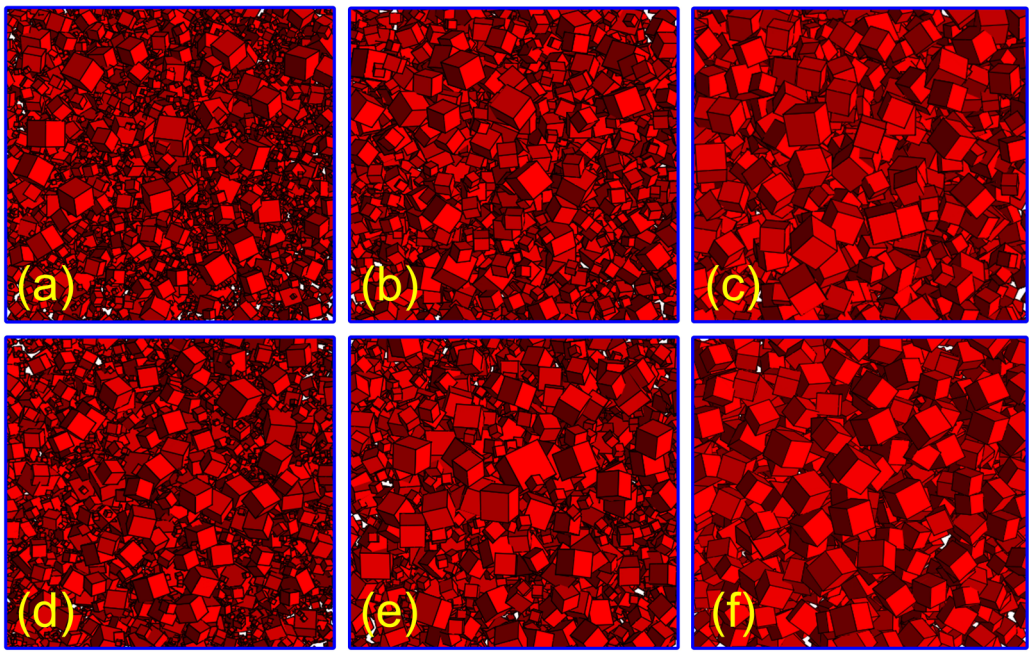

FIG. 3. Examples of the packings. Parts (a), (b), and (c) show packings with the Schulz distribution with, respectively, $m = 0$, 2, and 10, while parts (d), (e), and (f) present those generated with the log-normal PDF with standard deviations that are, respectively, $\sigma = 1$, 0.6, and 0.2.

Fig. 3. The results for other packing fractions are qualitatively similar to those that we present below.

We have computed the dependence of the particle density at the random close packing (RCP) on the parameter of m of the Schulz distribution and the standard deviation σ of the log-normal PDF. Moreover, we have also computed several of the most important microstructural descriptors of the packings for the same ranges of m and σ. In what follows, all the results were obtained with packings that contained at least 2 000 particles, while many of them were generated with up to 18 000 cubes. In addition, the results represent averages over at least 10 realizations of each packing.

A. Random close-packing fraction

Before we present and discuss the results for the random close-packing (RCP) fraction, we should point out that the value of the RCP fraction depends on the method or protocol by which a packing is generated. Thus, the RCP fraction is not unique. On the other hand, the jammed state of a packing is unique [50,51], and it has to do with the mechanical stability of the packing. In fact, the jammed state of a packing of soft cubic particles has been recently studied [52].

It is well known [7,11,13–17,19,21,24,25,27,40] that increasing the polydispersivity increases the packing efficiency because smaller particles pack more compactly by filling the voids between adjacent large particles. Some expressions for the packing fraction of polydisperse hard spheres that depend on the parameters of the particle-size distributions used [19,20], as well as some limits for their RCP [27] fractions, have previously been reported. The highest achievable packing fraction of polydisperse hard spheres is still unknown because, as pointed out earlier, the RCP fraction depends on the method by which one generates the packings [19]. Indeed, the maximum packing fraction of the structures generated by the RSA algorithm is different from those generated by the growth [14] and the shrinking cell [21] algorithms.

Using extensive simulations, we computed the packing density at the RCP point as a function of the Schulz distribution's polydispersivity parameter $m \in [0,10]$ and the standard deviation of the log-normal PDF, $\sigma \in [0,1]$. The results are shown in Fig. 4. While the maximum packing fraction for the most polydisperse packing generated by the Schulz distribution—the limit $m = 0$—is around 0.81, the corresponding estimate for the log-normal distribution is 0.71, obtained with $\sigma = 1$. Moreover, the packing fraction is as large as $\phi_{\mathrm{RCP},0} + (1 - \phi_{\mathrm{RCP},0})\phi_{\mathrm{RCP},0} \approx 0.82$ for a bidisperse packing with the size ratio $D_1/D_2 \to 0$. In the monodisperse limit, i.e., $m \to \infty$ or $\sigma \to 0$, the close-packing density for both distributions approaches the maximum packing fraction of the monodisperse packing, $\approx$0.57, which we calculated in parts I and II (see also Refs. [53–56], as well as the discussions below for monosized nonspherical particles). For example, the maximum packing fractions for $\sigma = 0.1$ and $m = 100$ are both close to 0.58. Moreover, while the close-packing density appears to vary linearly with $\sigma \in [0,1]$, it has a very sharp negative slope for $m \in [0,1]$ and varies slightly for $m \geqslant 3$.

Note that the maximum packing fraction for packings of polydisperse hard spheres is $\approx$0.75 if their size distribution is log-normal with $\sigma = 0.6$ [57], which should be compared with 0.64 [58] for random monodisperse packing of hard spheres. The approximate formula given by Desmond and Weeks [19] is also applicable only to close-packing densities with $\sigma \in [0,0.6]$. Note that the trends in Fig. 4(b) indicating that the maximum random close-packing fraction increases with the standard deviation of the log-normal distribution is consistent with the reported experimental data reported by Brouwers [59] (see also Ref. [60]).

Yu *et al.* [50] studied packings of nonspherical particles, and they presented an approximate formula based on the Westman

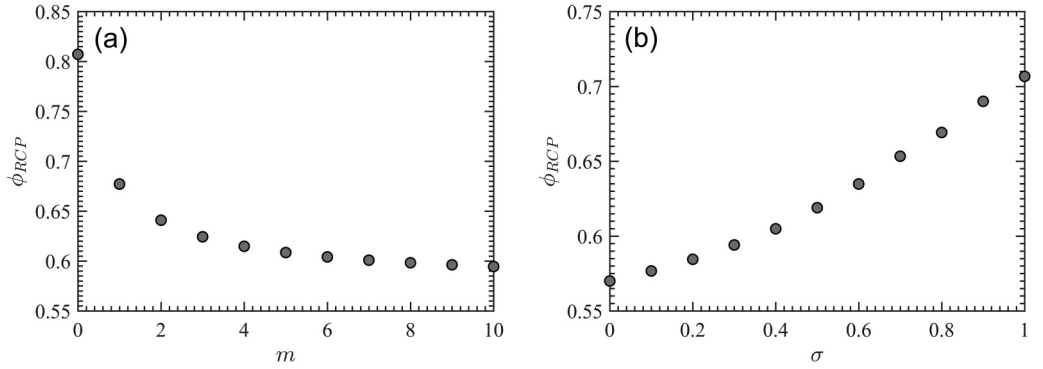

FIG. 4. Random close-packing density vs (a) the polydispersivity parameter m of the Schulz distribution, and (b) the standard deviation σ of the log-normal PDF.

equation [61] for the porosity of a binary mixture of such particles with intermediate size ratio D_1/D_2. For this purpose, they approximated nonspherical particles with spherical ones by introducing an "equivalent packing diameter," and they studied the porosity as a function of the volume fraction and size ratio of small and large particles. Good agreement was found between the empirical equation and experimental data.

B. Radial distribution function and the structure factor

One of the most important microstructural descriptors for packings of polydisperse particles (and for any material for that matter) is the radial distribution function $g(r)$, defined as the probability of finding a cube's centroid at a distance r from a given reference cube's centroid at the origin. Thus, $g(r)$ describes how the density of the packing varies as a function of r:

$$g(r) = \frac{\langle n(r)\rangle}{\rho v_s}, \tag{10}$$

where ρ is the total number density of the particles, and $\langle n(r)\rangle$ is the average number of particles in a spherical shell of volume v_s at a radial distance r from a reference cube's centroid. The importance of the radial distribution function is due to the fact that it can be determined experimentally by x-ray or neutron scattering via the structure factor $S(k)$, which for isotropic materials is given by [62–64]

$$S(k) = 1 + \frac{4\pi\rho}{k}\int_0^\infty \sin(kr)[g(r) - 1]r\,dr, \tag{11}$$

where k is the magnitude of the scattering wave vector. If there is no long-range order in the system, $g(r)$ and $S(k)$ decay to unity very rapidly as $r \to \infty$.

Figure 5 presents the average radial distribution function for several values of m, the Schulz distribution polydispersivity parameter, and σ, the standard deviation of the log-normal PDF. Also shown are the corresponding results for the monodisperse packings. The average $g(r)$ is a measure of the packing's structure, regardless of the cubes' diameters. A similar function was introduced by Stapleton *et al.* [65] for polydisperse Lennard-Jones fluids represented by spherical particles. For narrow symmetric size distributions, e.g., for $m = 10$ and $\sigma = 0.2$, $g(r)$ is very similar to that of monodisperse packings with the same packing fraction [5,6]. As the size distribution of the particles is broadened with higher skewness, the first peak of $g(r)$ and its oscillations beyond the peak are suppressed. Moreover, for higher degrees of polydispersivity, the first peak of $g(r)$ occurs at smaller distances r. Unlike the monodisperse packings [5,6] for which $g(r)$ has its first peak at $r \simeq 1.3D$ and essentially vanishes for radial distances less than $1.3D$, the polydisperse packings are characterized by radial distribution functions that vary continuously, starting from zero, until they reach their first peak. For example, for the most

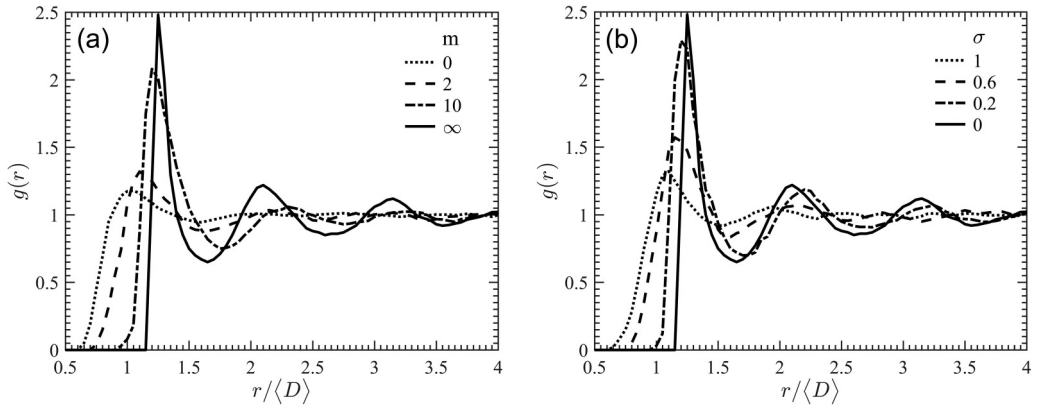

FIG. 5. Dependence of the radial distribution function $g(r)$ on (a) the polydispersivity parameter m of the Schulz distribution, and (b) the standard deviation σ of the log-normal distribution. $m = \infty$ and $\sigma = 0$ represent the monodisperse packings.

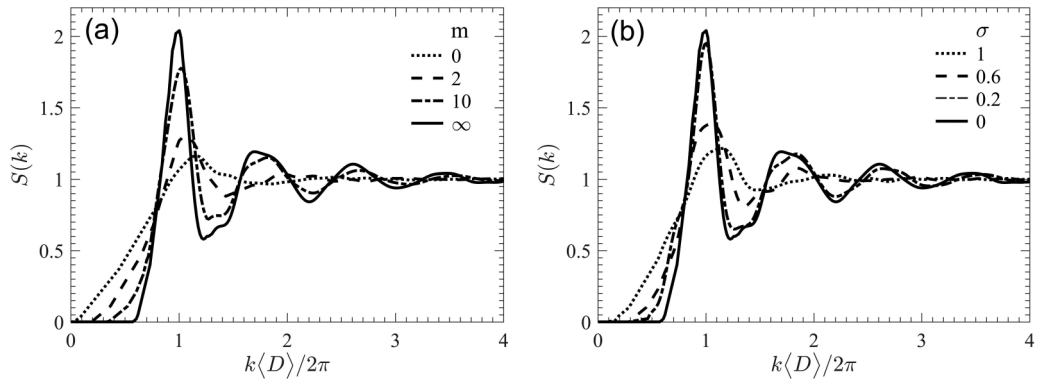

FIG. 6. Dependence of the structure factor $S(k)$ on (a) the polydispersivity parameter m of the Schulz distribution, and (b) the standard deviation σ of the log-normal distribution. $m = \infty$ and $\sigma = 0$ represent the monodisperse packings.

polydisperse packing generated by the Schulz distribution (the limit $m = 0$), $g(r)$ is nonzero at $r \simeq 0.6\langle D\rangle$, and it achieves its first peak at $r \leqslant \langle D\rangle$.

Figure 6 presents the structure factor $S(k)$ for the six packings of Fig. 3, calculated via Fourier transforming of $g(r)$, along with those for the monodisperse packings. Another way of computing $S(k)$ is by direct Fourier transforming of the particles' positions $\mathbf{r}_j$, leading to $S(\mathbf{k}) = |\sum_{j=1}^{N} \exp(i\mathbf{k}_j \cdot \mathbf{r}_j)|^2/N$, where N is the total number of particles. That is, $S(k)$ is computed by averaging it over $k = |\mathbf{k}|$. As Fig. 6 indicates, similar to $g(r)$, the structure factor $S(k)$ of the polydisperse packings exhibits behavior similar to that of the monodisperse packings if the particle-size distribution is narrow (such as, for example, $m = 10$ and $\sigma = 0.2$ for, respectively, the Schulz and log-normal distributions). Stronger polydispersivity results, however, in the suppression of the first peak, followed by oscillations around unity and loss of the structure since the packings contain particles of all sizes. The first peak of $S(k)$ occurs at larger wave numbers k as the polydispersivity increases (decreasing m or increasing σ). All the radial distribution functions and the structure factors are, of course, finite and approach unity as $r \to \infty$. The peaks beyond the first one indicate the structured behavior of the packings (disorder to order). As is well known, sharper and stronger oscillations around unity indicate that the packings exhibit behavior closer to long-range order or quasicrystalline behavior.

C. Analytical approximation for the structure factor

An important unsolved problem is the derivation of a closed-form analytical formula for the structure factor of disordered materials. In the absence of the solution of the problem, analytical approximations have been proposed for $S(k)$. In particular, for the Percus-Yevick fluids represented by polydisperse hard spheres with a Schulz distribution of the particles' size, the following accurate approximation has been proposed [43,66,67]:

$$S(k) = [\rho P(k)]^{-1} I(k), \tag{12}$$

with $I(k)$ being the scattering intensity, and $P(k)$ representing the scattering amplitude, given by

$$P(k) = 16\pi^2 \int_0^\infty f(D) y^2(k, D) dD, \tag{13}$$

where, as before, ρ is the total number density of the particles, and $y(t) = \sin t - t\cos t$, with $t = kD/2$. $I(k)$, the scattering intensity, is given by [43,68]

$$I(k) = \rho\Bigg[\int_0^\infty f(D_\alpha) F_\alpha^2(k, D_\alpha) dD_\alpha + \int_0^\infty dD_\alpha \times \int_0^\infty dD_\beta f(D_\alpha) f(D_\beta) F_\alpha(k, D_\alpha) F_\beta(k, D_\beta) H_{\alpha\beta}(k)\Bigg]. \tag{14}$$

Here, $F_\alpha(k, D_\alpha)$ is the single-particle amplitude form, and $H_{\alpha\beta}(k) = (\rho_\alpha \rho_\beta)^{1/2} h_{\alpha\beta}(k)$, with ρ_α being the number density of particles of size fraction α. The functions $h_{\alpha\beta}$ are the Fourier transforms of the total correlation functions, and they have a simple mathematical form for the Percus-Yevick solutions of hard spheres [43,66,67]. To derive an expression for the single-particle form amplitude, it is assumed [43] that the distribution of the scattering contrast in the spherical particles can be partitioned in a core of radius $a_1 = p_1 a_M$, followed by a sequence of $M - 1$ concentric shells, with each extending to an outer radius of $a_i = p_i a_M$ with $p_M = 1$. Then [69],

$$F_\alpha(k, D_\alpha) = \frac{4\pi}{k^3} \sum_{i=1}^{M} n_{i,i+1} y(0.5 k p_i D_\alpha / p), \tag{15}$$

where $n_{i,i+1} = n_i - n_{i+1}$, with n_i being the electron density in the shell i, $p = 0.5 D_\alpha / a_M$, and the function $y(t)$ was given earlier. More details are given elsewhere [43,66,67].

Although the packings that we study are quite different from the Percus-Yevick fluids, we used Eqs. (12)–(15) to predict $S(k)$ for the packings with a Schulz particle-size distribution. The results are presented in Fig. 7, where they are compared with the predictions of Eq. (12). All the qualitative trends indicated by our computed $S(k)$ are similar to those predicted by Eq. (12). Note that one reason for the difference between the computed and predicted $S(k)$ for small k is due to Eq. (12) not being able to precisely predict the scattering intensity at zero angle at high packing fractions and for broad particle-size distributions [67].

D. Loss of structure

To quantitatively investigate the "loss of structure" or "loss of order" in the polydisperse packings relative to the

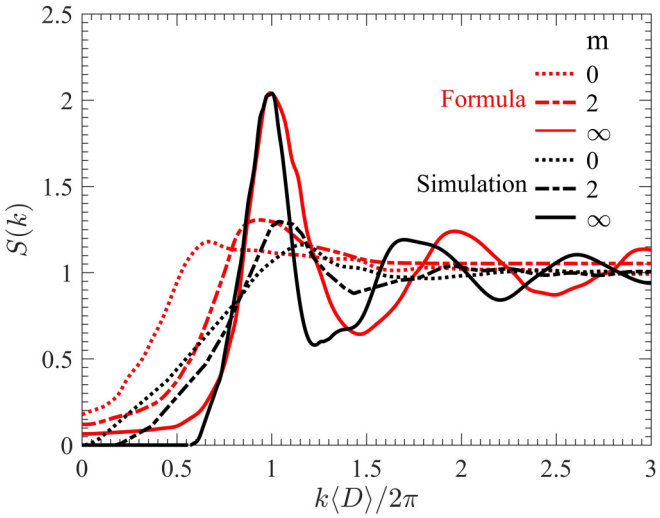

FIG. 7. Comparison of the structure factor $S(k)$, computed by the numerical simulation, and the predictions of the analytical approximation, Eq. (12). The sizes of the particles follow the Schulz distribution with the polydispersivity parameter m. The monodisperse packings correspond to $m = \infty$.

monodisperse ones, we use an order metric τ, introduced by Torquato *et al.* [70] and defined by

$$\tau \equiv \frac{1}{\ell^3}\int_0^\infty [g(\mathbf{r})-1]^2 d\mathbf{r} = \frac{1}{(2\ell\pi)^3\rho^2}\int_0^\infty [S(\mathbf{k})-1]^2 d\mathbf{k}, \tag{16}$$

where ℓ is some characteristic length scale, usually taken to be unity in order to rescale the configuration of the system and to make the number density ρ equal to unity [70]. The second equality in Eq. (12) is based on the use of Parseval's theorem. For spatially uncorrelated systems of particles—the "ideal gas"—$\tau = 0$ and, therefore, the deviation of τ from zero is a measure of order in the system. For perfectly crystalline structures, $\tau = \infty$.

Figure 8 presents the computed τ, with both the Schulz and log-normal distributions. The corresponding value of τ for the monodisperse packings at the same packing fraction of $\phi_2 = 0.2$ (see Fig. 3) is ≈13. Consider the results for, e.g., the Schulz distribution. As pointed out earlier, $m = 0$ corresponds to the highest degree of polydispersivity. Figure 8 indicates that τ is a monotonically increasing function of m, implying that the more polydisperse the packings are, the weaker are the correlations in the spatial distribution of the packings. That is, the more polydisperse the packings are, the closer they are to an "ideal gas," one for which $\tau = 0$. A similar trend is also indicated by Fig. 8 with a log-normal distribution of the particles' sizes.

E. Two-point probability function

Another important microstructural descriptor of a given phase i of a packing of particles is the two-point probability function $S_2^{(i)}(\mathbf{x}_1,\mathbf{x}_2)$, defined by

$$S_2^{(i)}(\mathbf{x}_1,\mathbf{x}_2) = \langle I^{(i)}(\mathbf{x}_1) I^{(i)}(\mathbf{x}_2)\rangle, \tag{17}$$

which represents the probability of finding two randomly selected points $\mathbf{x}_1$ and $\mathbf{x}_2$, separated by a distance r, belonging to phase i of a multiphase material. The indicator function is $I^{(i)}(\mathbf{x}) = 1$ if $\mathbf{x} \in$ phase i, and it is zero otherwise. For statistically homogeneous and isotropic media, $S_2^{(i)}(\mathbf{x}_1,\mathbf{x}_2)$ depends only on the distances, i.e.,

$$S_2^{(i)}(\mathbf{x}_1,\mathbf{x}_2) = S_2^{(i)}(r). \tag{18}$$

One also has $S_2^{(i)}(0) = \phi_i$, where ϕ_i is the volume fraction of phase i. In addition, $S_2^{(i)}$ must satisfy $\lim_{r\to\infty} S_2^{(i)}(r) \to \phi_i^2$. There are certain relations between $S_2^{(i)}$ and other microstructural descriptors [63,64], so that any knowledge about $S_2^{(i)}$ leads directly to information about such characteristics.

The computed $S_2^{(1)}(r)$ for the six packings of Fig. 3 are presented in Fig. 9, along with those for the monodisperse packings. Since the porosity ϕ_1 of all the packings equals 0.8, $S_2^{(1)}(0) \simeq 0.8$. Furthermore, $S_2^{(1)}(r)$ approaches 0.64 for large r since, theoretically, $\lim_{r\to\infty} S_2^{(1)}(r) = \phi_1^2$. The approaching rate to ϕ_1^2 is, however, different for various degrees of polydispersivity. The lower the degree of polydispersivity, the faster is the approaching rate. For the highest degree of polydispersivity, $m = 0$ in the Schulz distribution, $S_2^{(1)}(r)$ approaches ϕ_1^2 at radial distances $r > 5\langle D\rangle$. Thus, the probability of finding two points separated by a distance r in the pore space of a polydisperse packing is greater than that in a monodisperse packing with the same porosity or packing fraction.

In addition, $S_2^{(1)}(r)$ has a minimum at $r = \langle D\rangle$ for the narrowest polydispersivity that we studied, namely for $m = 10$

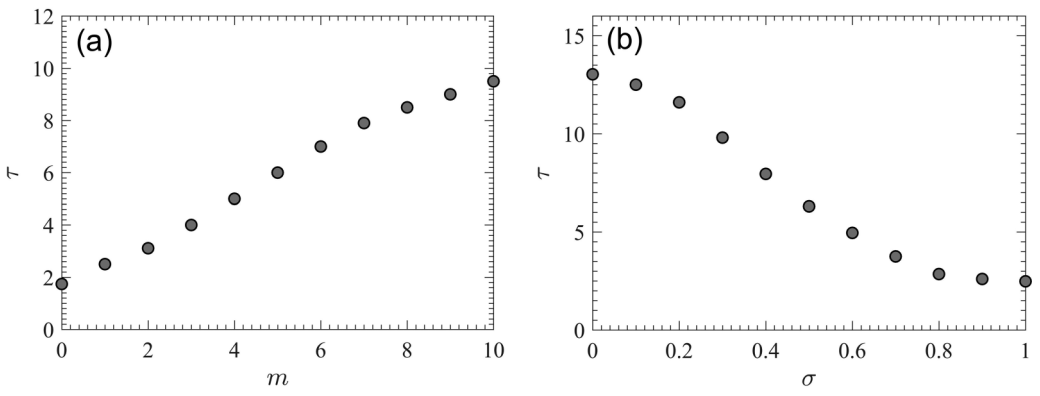

FIG. 8. Loss of order in the polydisperse packings, as characterized by the order metric τ defined by Eq. (12).

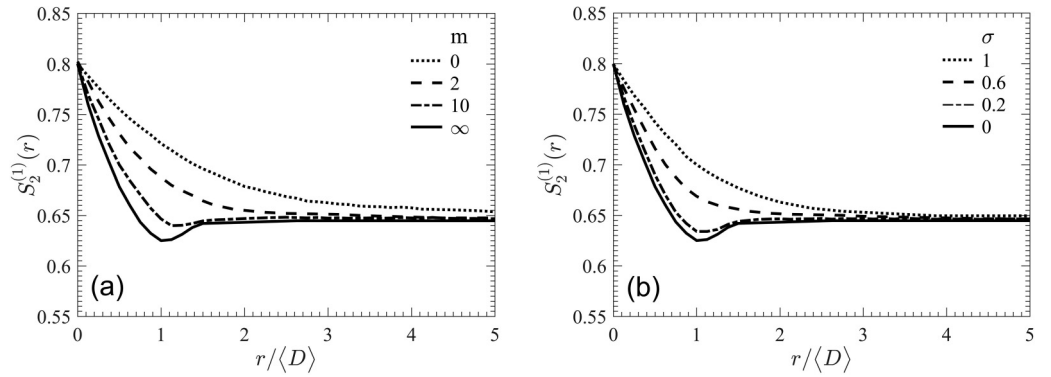

FIG. 9. Dependence of the two-point probability function $S_2^{(1)}(r)$ for the pore space of the packings on (a) the polydispersivity parameter m of the Schulz distribution, and (b) the standard deviation σ of the log-normal PDF. $m = \infty$ and $\sigma = 0$ represent the monodisperse packings.

and $\sigma = 0.2$ in the two particle-size distributions. This implies that in the monodisperse packings, the probability of finding in the pore space two end points of a line segment r, which is equal to the linear size of the cubes, is lower than any other distance r. Thus, we may deduce that, compared with the monodisperse packings, the polydisperse ones contain more connected void space. This feature, which is more distinctive for higher degrees of polydispersivity, affects the flow and transport properties of such packings.

F. Specific surface

The specific surface s, defined as the interfacial area per unit volume, contains information about the internal surface of porous media. For the packings under study, s is computed by

$$s = 6\eta \frac{\langle D^2\rangle}{\langle D^3\rangle}, \tag{19}$$

where $\eta = \rho\langle D^3\rangle$ is the reduced density of the system, equivalent to ϕ_2. The surface area ratio A is the ratio of the specific surface of a polydisperse system and that of a monodisperse one with the same packing fraction ϕ_2. Figure 10 presents the quantity versus m, the polydispersivity parameter of the Schulz distribution, and σ, the standard deviation of the log-normal PDF. In both cases, A decreases with increasing polydispersivity, implying that the more dispersed the packings are, the smaller is the specific surface they possess, which is due to filling up the small holes between the large particles with smaller ones.

G. Lineal-path function

A very useful statistical characteristic of random packings of solid objects is their lineal-path function $L^{(i)}(z)$, the probability of finding a randomly thrown line segment of length z entirely in phase i. Since $L^{(i)}(z)$ quantifies connectedness along a lineal path, it is also known as the coarse-scale connectedness function. Its limiting values are $L^{(i)}(0) = \phi_i$ and $L^{(i)}(\infty) = 0$. In the limit $z = 0$ one has, $L^{(1)}(0) = \phi_1$, the porosity of the packing, whereas the tail of the function as $z \to \infty$ yields information about the largest possible line segment in the packing's pore space.

Figure 11 presents the lineal function for the six packings, three each with the Schulz and log-normal distributions. For both distributions, the higher the degree of polydispersivity, the more likely it is to find a line segment of length z entirely in the pore phase. The longest possible line segment entirely in the pore space belongs to the packing with the highest degree of polydispersivity, the limit $m = 0$ in the Schulz distribution. The maximum possible length of a line segment in the pore space is a bit larger than $0.8\langle D\rangle$. For the monodisperse packings, represented by the limits $m \to \infty$ and $\sigma = 0$ in the two particle-size distributions, the maximum length of a line segment entirely in the void space is around $z \approx 0.4\langle D\rangle$, almost half of that for the highest degree of polydispersivity.

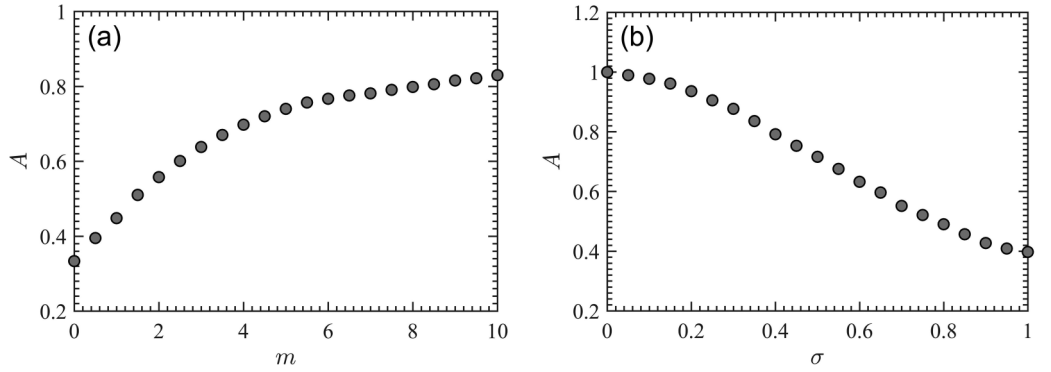

FIG. 10. The surface area ratio A vs (a) the polydispersivity parameter m of the Schulz distribution, and (b) the standard deviation σ of the log-normal PDF.

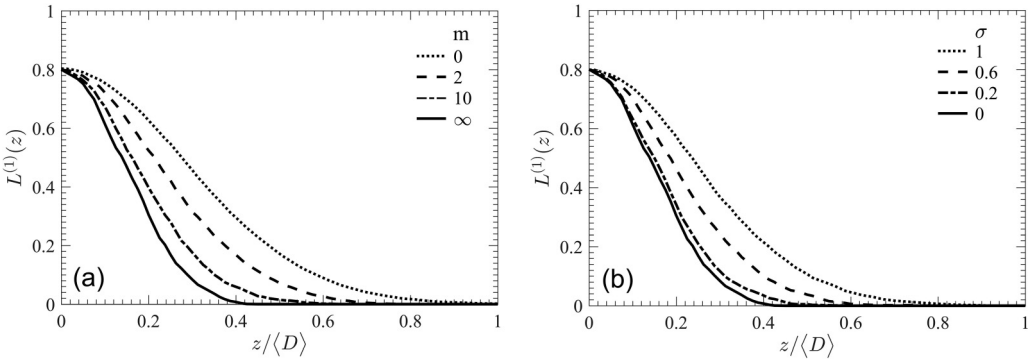

FIG. 11. Dependence of the lineal-path function $L^{(1)}(z)$ of the pore space of the packings on (a) the polydispersivity parameter m of the Schulz distribution, and (b) the standard deviation σ of the log-normal distribution. $m = \infty$ and $\sigma = 0$ represent the monodisperse packings.

This provides further evidence that the polydisperse packings contain more connected pore space than the monodisperse ones.

H. Pore-size distribution

The pore-size distribution function $P(\delta)$ of a porous medium is defined such that $P(\delta)d\delta$ is the probability that a randomly selected point in the pore phase is at a distance between δ and $\delta + d\delta$ from the nearest point at the pore-solid interface. Thus, $P(\delta)$ is related to the probability of inserting a sphere of radius δ into the system. Since $P(\delta)$ is a probability density function, it normalizes to unity, i.e., $\int_0^\infty P(\delta)d\delta = 1$. Note that $P(\delta)$ is not the same as the classical pore-size distribution that is used to quantify the statistical distribution of the effective sizes of the pore bodies and pore throats in a pore space, which is measured by a variety of techniques [71]. The associated cumulative distribution function $F(\delta)$ represents the fraction of the pore space that has a pore radius larger than δ:

$$F(\delta) = \int_\delta^\infty P(r)dr. \tag{20}$$

Hence, the limiting values of $F(\delta)$ are $F(0) = 1$ and $F(\infty) = 0$. The mean pore size $\langle\delta\rangle$ is then given by

$$\langle\delta\rangle = \int_0^\infty \delta P(\delta)d\delta = \int_0^\infty F(\delta)d\delta. \tag{21}$$

Figure 12 illustrates the cumulative pore-size distributions $F(\delta)$, computed for the six packings of Fig. 3. For both particle-size distributions, the area under the $F(\delta)$ curves is greater for higher degrees of polydispersivity, implying that the mean pore size $\langle\delta\rangle$ in the polydisperse packings is greater than that of the monodisperse one. While the largest pore size is around $\approx 1.75\langle\delta\rangle$ for the highest degree of polydispersivity with the Schulz distribution, it is around $\approx 0.75\langle\delta\rangle$ for $\sigma = 0.2$ in the log-normal distribution. This is due to the fact that the long tail of the log-normal distribution generates some very large particles that can be better filled up by very small particles, hence reducing the pore sizes.

I. Mean survival time and principal relaxation time

Two other important physical quantities are closely related to the cumulative distribution $F(\delta)$. One is the mean survival time T_m of a diffusing species that undergoes a first-order reaction among partially absorbing traps in the porous medium that a packing represents. A lower bound to T_m is given by [72,73]

$$T_m \geqslant \frac{1}{\ell}\left(\int_0^\infty F(\delta)d\delta\right)^2. \tag{22}$$

The second property is the principal relaxation time T_1 in the same diffusion problem, which also arises in the problem of the relation between nuclear magnetic resonance and the effective permeability of a porous medium [68,74–76], with

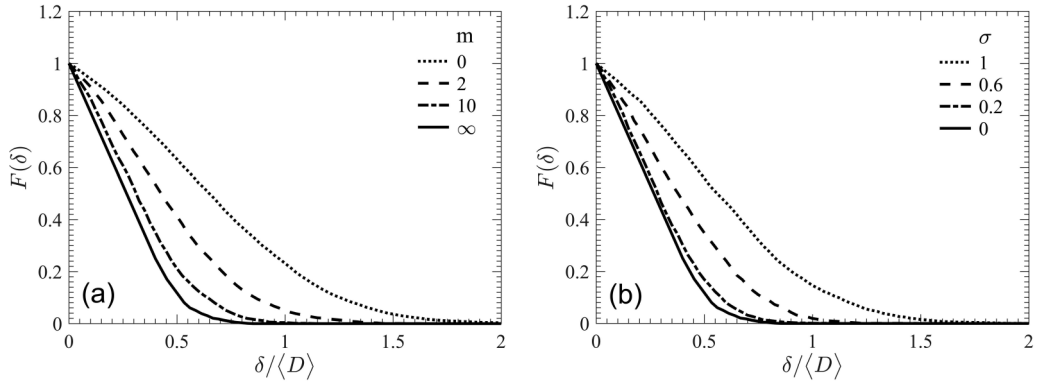

FIG. 12. Dependence of the cumulative pore-size distribution function $F(\delta)$ on (a) the polydispersivity parameter m of the Schulz distribution, and (b) the standard deviation σ of the log-normal distribution. $m = \infty$ and $\sigma = 0$ represent the monodisperse packings.

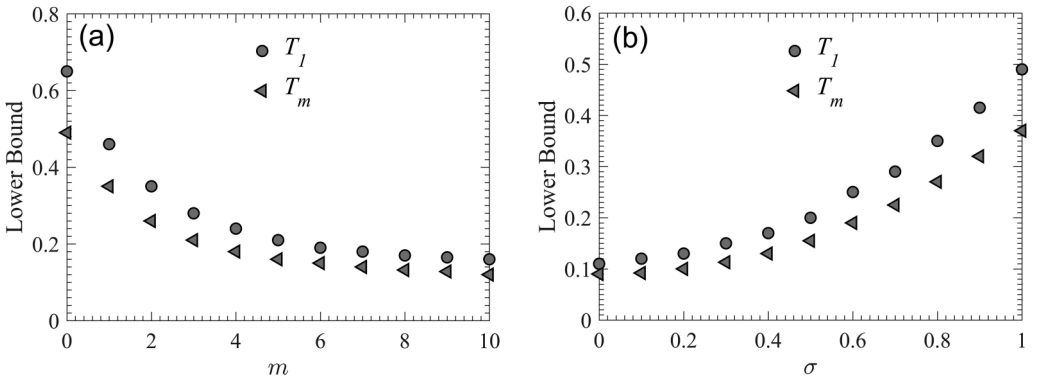

FIG. 13. Lower bounds for the mean survival time T_m and the principal relaxation time T_1 of a diffusing species in the two types of packings.

the permeability K given by $K \propto T_1^f$ with $f \approx 2$ [71]. The following rigorous lower bound has been derived for T_1 [72,73]:

$$T_1 \geqslant \frac{2}{\ell} \int_0^\infty \delta F(\delta) d\delta, \tag{23}$$

where, as previously mentioned, ℓ is usually taken to be unity.

The computed lower bounds for T_m and T_1 are presented in Fig. 13. According to Fig. 13, the monodisperse packings have the shortest survival and relaxation times, but the times increase as the polydispersivity of the packings increases. The reason is due to the nature of the reaction-diffusion phenomenon: Absorbing traps in a packing with equal-size particles in which a species diffuses cannot be avoided for a long time, since the diffusion paths are not too tortuous. On the other hand, as the packings become more polydisperse, smaller particles fill up the pores between the large particles, hence providing more tortuous diffusion paths for the species, implying that it takes longer to encounter the traps and be absorbed by them.

J. Nearest-neighbor functions

The particle nearest-neighbor probability density function $H_P(r)$ is defined such that $H_P(r)dr$ is the probability of finding the nearest-neighbor particle's center at a distance between r and $r + dr$ from an arbitrary reference particle's center in the packing. A second nearest-neighbor function, $H_V(r)$, referred to as the void nearest-neighbor PDF, is defined in a similar manner, i.e., $H_V(r)dr$ is the probability of finding the nearest-neighbor particle's center at a distance between r and $r + dr$ from an arbitrary point in the void region of the system. While the first moment of $H_V(r)$ is related to that of the pore-size function $P(\delta)$, the first moment of $H_P(r)$ yields the mean nearest-neighbor distance l_P between the particles:

$$l_P = \int_0^\infty r H_P(r) dr. \tag{24}$$

To compare the results with those for the monodisperse packings, we define L_P as the ratio of the mean nearest-neighbor distance of a polydisperse system and that of a monodisperse packing with the same packing fraction ϕ_2 (or porosity ϕ_1). Figure 14 presents the dependence of L_P on the polydispersivity parameter m of the Schulz distribution, and on σ, the standard deviation of the log-normal PDF. In both cases, the scaled mean nearest-neighbor distance decreases upon increasing the degree of polydispersivity because smaller particles can fill the void space between the large ones, hence decreasing L_P. With the Schulz distribution, L_P varies from 0.35 for the highest degree of polydispersivity (i.e., for $m = 0$) to around 0.8 for the narrowest distribution. It approaches unity with a slight tilt as m increases. With the log-normal distribution, on the other hand, L_P varies from unity for the monodisperse packing (i.e., for $\sigma = 0$) to around 0.48 for the most polydisperse system that we simulated. The implications are clear: (i) The distances between nearest-neighbor particles

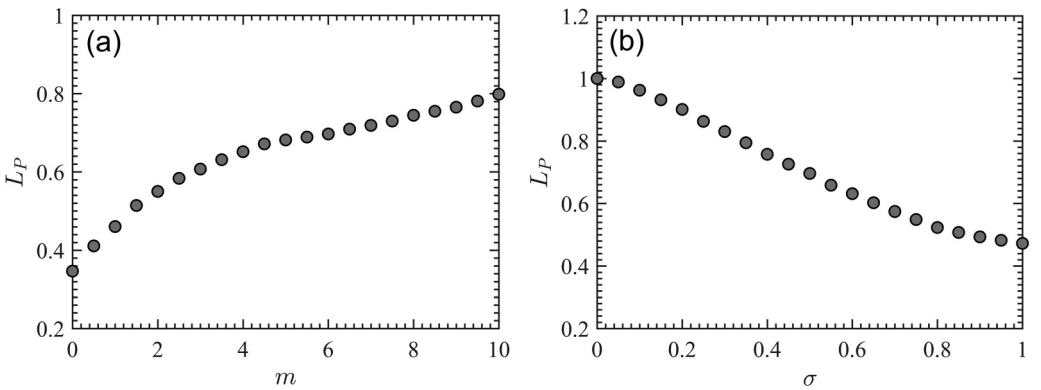

FIG. 14. The scaled mean nearest-neighbor distance L_P vs (a) the polydispersivity parameter m of the Schulz distribution, and (b) the standard deviation σ of the log-normal PDF.

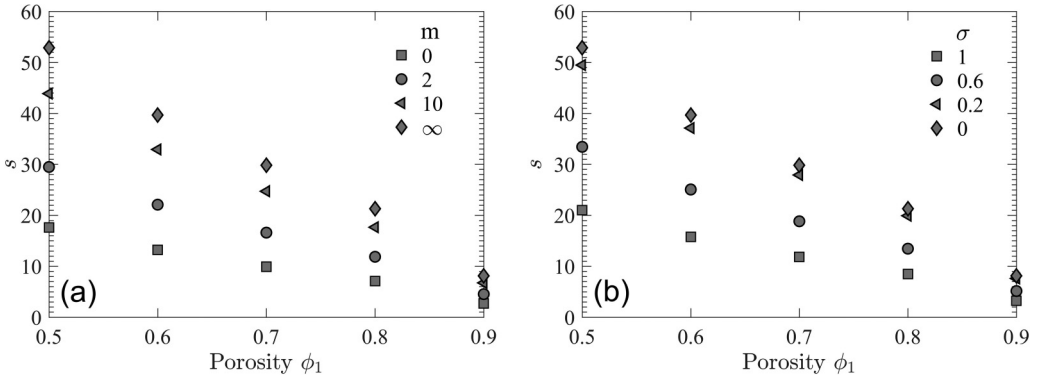

FIG. 15. Dependence of the specific surface area s on the porosity for various values of (a) the polydispersivity parameter m of the Schulz distribution, and (b) the standard deviation σ of the log-normal PDF. $m = \infty$ and $\sigma = 0$ represent the monodisperse packings.

in the polydisperse packings are considerably less than those in the monodisperse packings, and (ii) due to the long tail of the log-normal distribution that gives rise to some very large cubes, the distances between the nearest-neighbor particles with a log-normal particle-size distribution are smaller than those in the packing with a Schulz distribution. In other words, the presence of very large cubes also creates very large voids in between the particles that are filled by multiple small particles, hence reducing the distance between nearest-neighbor particles.

K. Effect of porosity

All the results presented so far were for packings with a fixed porosity of $\phi_1 = 0.8$. In this section, we present the porosity dependence of two important properties, namely the specific surface area s and the mean nearest-neighbor distance l_p between the particles. Figure 15 presents the dependence of s on the porosity ϕ_1 of the packings with the two types of particle-size distribution. As the porosity decreases, the interfacial area between the particles increases, since the distance between them decreases. Moreover, upon increasing the degree of polydispersivity at a fixed porosity, the interfacial area decreases since, once again, the small particles fill up the void between the large ones. The trends are identical for both types of particle-size distribution. In addition, for any m and σ, which are the parameters of the two distributions, the specific surface area depends on the porosity more or less linearly, which is then useful for estimating s for any other porosity.

Figure 16 presents the results for the nearest-neighbor distance l_p. Clearly, as the porosity increases, so also should l_p as the void space expands at higher ϕ_1. The expectation is confirmed by the results shown in Fig. 16 for both particle-size distributions. Similar to the specific surface area s, the nearest-neighbor distance l_p varies linearly with the porosity. The linear dependence of s and l_p on the porosity is the direct result of the nonoverlapping constraint that we have imposed on the particles. If the particles are allowed a degree of overlap—the so-called *cherry-pit* model [63,64]—the linear dependence should disappear and be replaced by a more complex dependence.

IV. SUMMARY

This paper reports on the statistical characterization of the microstructure of packings of nonoverlapping polydisperse cubic particles. Two types of particle-size distributions, namely the Schulz and log-normal distributions, were utilized, and the random close packing density of the porous media was computed for various degrees of polydispersivity. In addition, some of the most important microstructural descriptors, including the radial distribution function and the corresponding structure factor, the two-point probability function, the specific surface and lineal-path function, as well as the pore-size

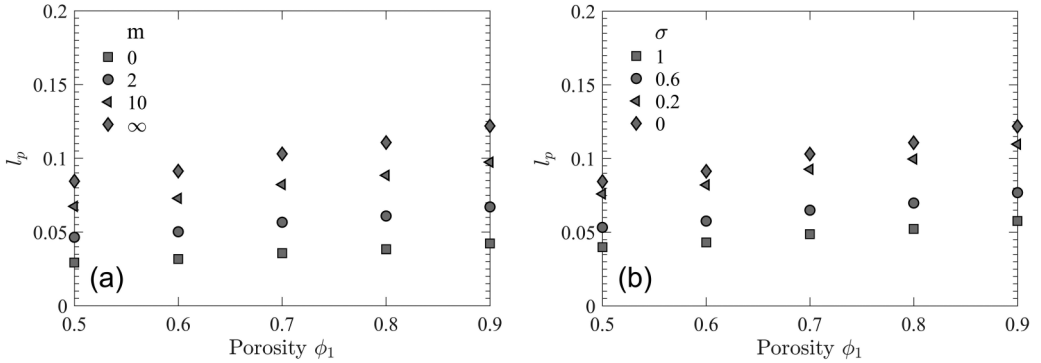

FIG. 16. Dependence of the mean nearest-neighbor distance l_p on the porosity of the packings for several values of (a) the polydispersivity parameter m of the Schulz distribution, and (b) the standard deviations σ of the log-normal PDF. $m = \infty$ and $\sigma = 0$ represent the monodisperse packings.

and nearest-neighbor functions, were calculated and analyzed for numerous degrees of polydispersivity. With the Schulz distribution with the highest degree of polydispersivity the maximum packing fraction is computed to be about 0.81, whereas the corresponding value computed with the log-normal particle-size distribution with a standard deviation $\sigma \in [0,10]$ is about 0.71, computed with $\sigma = 1$.

Furthermore, it was demonstrated that the probability of finding two points separated by a distance r in the pore space of a polydisperse packing is greater than that in a monodisperse one with the same porosity. The maximum length of a line segment entirely in the void space of a packing with the largest degree of polydispersivity, as well as the maximum pore size in the same packing, are twice those of a monodisperse packing. Hence, polydisperse packings contain better connected void space. Their specific surface areas are also smaller than the corresponding value in monodisperse packings.

More importantly, we showed that (i) an approximate analytical expression for the structure factor of Percus-Yevick fluids of polydisperse hard spheres in which the particles' sizes follow a Schulz distribution also predicts all the qualitative features of the structure factor of the packings that have been studied in this paper; (ii) as the packings become more polydisperse, their behavior resembles increasingly that of an ideal system—"ideal gas"—with little or no correlations; and (iii) the mean survival time and mean relaxation time of a diffusing species in the packings increase with higher degrees of polydispersivity.

ACKNOWLEDGMENTS

Work at the University of Southern California was supported in part by the Petroleum Research Fund, administered by the American Chemical Society.

[1] A. R. Mehrabi, L. Vaziri, R. Mehrabi, J. M. de Santos, and M. Sahimi, Novel method for fabrication of porous materials with controlled morphology, Adv. Mater. (unpublished).
[2] Z. A. Almsherqi, S. D. Kohlwein, and Y. Deng, Cubic membranes: A legend beyond the Flatland of cell membrane organization, J. Cell Biol. **173**, 839 (2006).
[3] L. Rossi, S. Sacanna, W. T. M. Irvine, P. M. Chaikin, D. J. Pine, and A. P. Philipse, Cubic crystals from cubic colloids, Soft Matter **7**, 4139 (2011).
[4] M. Norouzi Rad, N. Shokri, and M. Sahimi, Pore-scale dynamics of salt precipitation in drying porous media, Phys. Rev. E **88**, 032404 (2013).
[5] H. Malmir, M. Sahimi, and M. R. Rahimi Tabar, Microstructural characterization of random packings of cubic particles, Sci. Rep. **6**, 35024 (2016).
[6] H. Malmir, M. Sahimi, and M. R. Rahimi Tabar, Packing of nonoverlapping cubic particles: Computational algorithms and microstructural characteristics, Phys. Rev. E **94**, 062901 (2016).
[7] E. Dickinson, Polydisperse suspensions of spherical colloidal particles: Analogies with multicomponent molecular liquid mixtures, Ind. Eng. Chem. Prod. Res. Dev. **25**, 82 (1986).
[8] A. P. Shapiro and R. F. Probstein, Random Packings of Spheres and Fluidity Limits of Monodisperse and Bidisperse Suspensions, Phys. Rev. Lett. **68**, 1422 (1992).
[9] B. Lu and S. Torquato, General formalism to characterize the microstructure of polydispersed random media, Phys. Rev. A **43**, 2078 (1991).
[10] B. Lu and S. Torquato, Nearest-surface distribution functions for polydispersed particle systems, Phys. Rev. A **45**, 5530 (1992).
[11] Z. Adamczyk, B. Siwek, M. Zembala, and P. Weronski, Influence of polydispersity on random sequential adsorption of spherical particles, J. Colloid Interface Sci. **185**, 236 (1997).
[12] A. Daneyko, A. Höltzel, S. Khirevich, and Ul. Tallarek, Influence of the particle size distribution on hydraulic permeability and eddy dispersion in bulk packings, Anal. Chem. **83**, 3903 (2011).
[13] D. He, N. N. Ekere, and L. Cai, Computer simulation of random packing of unequal particles, Phys. Rev. E **60**, 7098 (1999).
[14] A. R. Kansal, S. Torquato, and F. H. Stillinger, Computer generation of dense polydisperse sphere packings, J. Chem. Phys. **117**, 8212 (2002).
[15] H. J. H. Brouwers, Particle-size distribution and packing fraction of geometric random packings, Phys. Rev. E **74**, 031309 (2006).
[16] Y. Shi and Y. Zhang, Simulation of random packing of spherical particles with different size distributions, Appl. Phys. A **92**, 621 (2008).
[17] R. S. Farr and R. D. Groot, Close packing density of polydisperse hard spheres, J. Chem. Phys. **131**, 244104 (2009).
[18] E. I. Corwin, M. Clusel, A. O. N. Siemens, and J. Brujic, Model for random packing of polydisperse frictionless spheres, Soft Matter **6**, 2949 (2010).
[19] K. W. Desmond and E. R. Weeks, Influence of particle size distribution on random close packing of spheres, Phys. Rev. E **90**, 022204 (2014).
[20] C. Zhang, C. B. O'Donovan E. I. Corwin, F. Cardinaux, T. G. Mason, M. E. Mobius, and F. Scheffold, Structure of marginally jammed polydisperse packings of frictionless spheres, Phys. Rev. E **91**, 032302 (2015).
[21] D. Chen and S. Torquato, Confined disordered strictly jammed binary sphere packings, Phys. Rev. E **92**, 062207 (2015).
[22] D. Hlushkou, H. Liasneuski, U. Tallarek, and S. Torquato, Effective diffusion coefficients in random packings of polydisperse hard spheres from two-point and three-point correlation functions, J. Appl. Phys. **118**, 124901 (2015).
[23] W. Schaertl and H. Sillescu, Brownian dynamics of polydisperse colloidal hard spheres: Equilibrium structures and random close packings, J. Stat. Phys. **77**, 1007 (1994).
[24] S. I. Henderson, T. C. Mortensen, S. M. Underwood, and W. van Megen, Effect of particle size distribution on crystallisation and the glass transition of hard sphere colloids, Physica A **233**, 102 (1996).
[25] S.-E. Phan, W. B. Russel, J. Zhu, and P. M. Chaikin, Effects of polydispersity on hard sphere crystals, J. Chem. Phys. **108**, 9789 (1998).
[26] C. E. Zachary, Y. Jiao, and S. Torquato, Hyperuniformity, quasi-long-range correlations, and void-space constraints in maximally random jammed particle packings. I. Polydisperse spheres, Phys. Rev. E **83**, 051308 (2011).
[27] V. Baranau and U. Tallarek, Random-close packing limits for monodisperse and polydisperse hard spheres, Soft Matter **10**, 3826 (2014).

[28] J. F. Thovert, I. C. Kim, S. Torquato, and A. Acrivos, Bounds on the effective properties of polydispersed suspensions of spheres: An evaluation of two relevant morphological parameters, J. Appl. Phys. **67**, 6088 (1990).
[29] Y. Li and C.-W. Park, Permeability of packed beds filled with polydisperse spherical particles, Ind. Eng. Chem. Res. **37**, 2005 (1998).
[30] S. Deridder and G. Desmet, Calculation of the geometrical three-point parameter constant appearing in the second order accurate effective medium theory expression for the B-term diffusion coefficient in fully porous and porous-shell random sphere packings, J. Chromatogr. A **1223**, 35 (2012).
[31] N. Rangnekar, N. Mittal, B. Elyassi, J. Caro, and M. Tsapatsis, Zeolite membranes: A review and comparison with MOFs, Chem. Soc. Rev. **44**, 7128 (2015).
[32] S. M. Auerbach, K. A. Carrado, and P. K. Dutta, *Handbook of Zeolite Science and Technology* (CRC, Baton Rouge, LA, 2003).
[33] C. D. Cwalina, K. J. Harrison, and N. J. Wagner, Rheology of cubic particles suspended in a Newtonian fluid, Soft Matter **12**, 4654 (2016).
[34] P. Sharma, J.-S. Song, M. H. Han, and C.-H. Cho, GIS-NaP1 zeolite microspheres as potential water adsorption material: Influence of initial silica concentration on adsorptive and physical/topological properties, Sci. Rep. **6**, P22734 (2016).
[35] B. D. Lubachevsky and F. H. Stillinger, Geometric properties of random disk packings, J. Stat. Phys. **60**, 561 (1990).
[36] M. Clusel, E. I. Corwin, A. O. N. Siemens, and J. Brujic, A "granocentric" model for random packing of jammed emulsions, Nature (London) **460**, 611 (2009).
[37] S. Torquato and Y. Jiao, Dense packings of polyhedra: Platonic and Archimedean solids, Phys. Rev. E **80**, 041104 (2009).
[38] Y. Jiao and S. Torquato, Maximally random jammed packings of Platonic solids: Hyperuniform long-range correlations and isostaticity, Phys. Rev. E **84**, 041309 (2011).
[39] G. W. Delaney and P. W. Cleary, The packing properties of superellipsoids, Europhys. Lett. **89**, 34002 (2010).
[40] P. J. Flory, Molecular size distribution in linear condensation polymers, J. Am. Chem. Soc. **58**, 1877 (1936).
[41] J. Welsh and V. A. Bloomfield, Fitting polymer distribution data to a Schulz-Zimm function, J. Polym. Sci. Polym. Phys. **11**, 1855 (1973).
[42] R. K. Pandey and D. N. Tripathi, Schulz distribution function and the polydispersity of the binary suspension of charged macroions, Coll. Surf. A **190**, 217 (2001).
[43] M. Nayeri, M. Zackrisson, and J. Bergenholtz, Scattering functions of core-shell-structured hard spheres with Schulz-distributed radii, J. Phys. Chem. B **113**, 8296 (2009).
[44] E. Limpert, W. A. Stahel, and M. Abbt, Log-normal distributions across the sciences: Keys and clues, BioScience **51**, 341 (2001).
[45] J. Söderlund, L. B. Kiss, G. A. Niklasson, and C. G. Granqvist, Lognormal Size Distributions in Particle Growth Processes without Coagulation, Phys. Rev. Lett. **80**, 2386 (1998).
[46] R. Chantrell, J. Popplewell, and S. Charles, Measurements of particle size distribution parameters in ferrofluids, IEEE Trans. Mag. **14**, 975 (1978).
[47] G. M. Kondolf and A. Adhikari, Weibull vs. lognormal distributions for fluvial gravels, J. Sedimentary Res. **70**, 456 (2000).
[48] C. Reimann and P. Filzmoser, Normal and lognormal data distribution in geochemistry: Death of a myth. Consequences for the statistical treatment of geochemical and environmental data, Environ. Geol. **39**, 1001 (2000).
[49] M. Madadi and M. Sahimi, Lattice Boltzmann simulation of fluid flow in fracture networks with rough, self-affine surfaces, Phys. Rev. E **67**, 026309 (2003).
[50] S. Torquato, T. M. Truskett, and P. G. Debenedetti, Is Random Close Packing of Spheres Well Defined? Phys. Rev. Lett. **84**, 2064 (2000).
[51] M. van Hecke, Jamming of soft particles: Geometry, mechanics, scaling and isostaticity, J. Phys.: Condens. Matter **22**, 033101 (2010).
[52] K. C. Smith, I. Srivastava, T. S. Fisher, and M. Alam, Variable-cell method for stress-controlled jamming of athermal, frictionless grains, Phys. Rev. E **89**, 042203 (2014).
[53] A. B. Yu, N. Standish, and A. McLean, Porosity calculation of binary mixtures of nonspherical particles, J. Am. Ceram. Soc. **76**, 2813 (1993).
[54] J. Baker and A. Kudrolli, Maximum and minimum stable random packings of platonic solids, Phys. Rev. E **82**, 061304 (2010).
[55] U. Agarwal and F. A. Escobedo, Mesophase behavior of polyhedral particles, Nat. Mater. **10**, 230 (2011).
[56] R. P. Zou and A. B. Yu, Evaluation of the packing characteristics of mono-sized non-spherical particles, Powder Technol. **88**, 71 (1996).
[57] H. Y. Sohn and C. Moreland, The effect of particle size distribution on packing density, Can. J. Chem. Eng. **46**, 162 (1968).
[58] G. D. Scott and D. M. Kilgour, The density of random close packing of spheres, J. Phys. D: Appl. Phys. **2**, 863 (1969).
[59] H. J. H. Brouwers, Packing fraction of particles with lognormal size distribution, Phys. Rev. E **89**, 052211 (2014).
[60] A. Yang, C. T. Miller, and L. D. Turcoliver, Simulation of correlated and uncorrelated packing of random size spheres, Phys. Rev. E **53**, 1516 (1996).
[61] A. E. R. Westman, The packing of particles: Empirical equation for intermediate diameter ratios, J. Am. Ceram. Soc. **19**, 127 (1936).
[62] J.-P. Hansen and I. R. McDonald, *Theory of Simple Liquids* (Elsevier, New York, 1990).
[63] S. Torquato, *Random Heterogeneous Materials* (Springer, New York, 2002).
[64] M. Sahimi, *Heterogeneous Materials I* (Springer, New York, 2003).
[65] M. R. Stapleton, D. J. Tildesley, T. J. Sluckin, and N. Quirke, Computer simulation of polydisperse liquids with density- and temperature-dependent distributions, J. Phys. Chem. **92**, 4788 (1988).
[66] P. van Beurten and A. Vrij, Polydispersity effects in the small-angle scattering of concentrated solutions of colloidal spheres, J. Chem. Phys. **74**, 2744 (1981).
[67] W. L. Griffith, R. Triolo, and A. L. Compere, Analytical scattering function of a polydisperse Percus-Yevick fluid with Schulz- (Γ-) distributed diameters, Phys. Rev. A **35**, 2200 (1987).
[68] L. Blum and G. Stell, Polydisperse systems. I. Scattering function for polydisperse fluids of hard or permeable spheres, J. Chem. Phys. **71**, 42 (1979); Polydisperse systems. I. Scattering function for polydisperse fluids of hard or permeable spheres, **72**, 2212 (1980).

[69] J. B. Hayter, in *Physics of Amphiphiles: Micelles, Vesicles and Microemulsions*, edited by V. Degiorgio and M. Corti (North-Holland, Amsterdam, 1985), p. 59.

[70] S. Torquato, G. Zhang, and F. H. Stillinger, Ensemble Theory for Stealthy Hyperuniform Disordered Ground States, Phys. Rev. X **5**, 021020 (2015).

[71] M. Sahimi, *Flow and Transport in Porous Media and Fractured Rock*, 2nd ed. (Wiley-VCH, Weinheim, 2011).

[72] S. Torquato and M. Avellaneda, Diffusion and reaction in heterogeneous media: Pore size distribution, relaxation times, and mean survival time, J. Chem. Phys. **95**, 6477 (1991).

[73] G. Zhang, F. H. Stillinger, and S. Torquato, Transport, geometrical, and topological properties of stealthy disordered hyperuniform two-phase systems, J. Chem. Phys. **145**, 244109 (2016).

[74] J. R. Banavar and L. M. Schwartz, Magnetic Resonance as a Probe of Permeability in Porous Media, Phys. Rev. Lett. **58**, 1411 (1987).

[75] W. E. Kenyon, P. I. Day, C. Straley, and J. F. Willemsen, Three-part study of NMR longitudinal relaxation properties of water-saturated sandstones, SPE Form. Eval. **3**, 622 (1988).

[76] A. H. Thompson, S. W. Sinton, S. L. Huff, A. J. Katz, R. A. Raschke, and G. A. Gist, Deuterium magnetic resonance and permeability in porous media, J. Appl. Phys. **65**, 3259 (1989).